Check for
updates

Plasma electrolytic oxidation (PEO) coating to enhance in vitro corrosion resistance of AZ91 magnesium alloy coated with polydimethylsiloxane (PDMS)

Negar Mehri Ghahfarokhi[1] · Behrooz Shayegh Broujeny[1] · Amin Hakimizad[2] · Ali Doostmohammadi[3]

Abstract

To improve the corrosion behavior of a magnesium alloy, two-step coatings have been fabricated through plasma electrolytic oxidation coating (PEO) under constant voltage conditions applied to the AZ91 substrate surface in the silicate electrolyte. A polymeric layer [Polydimethylsiloxane (PDMS)] has been successfully implemented by the immersion method on both bare AZ91 alloy and pre-treated samples by the PEO process. PEO coating contains MgO, $MgSiO_3$, and Mg_2SiO_4 phases detected by X-ray diffraction patterns (XRD). The surface morphology observation investigated using the field emission scanning electron microscopy (FESEM) showed a porous and non-porous layer on the substrate for PEO and PEO/PDMS coatings, respectively. The topography and roughness of the PEO coating evaluated by atomic force microscopy (AFM) revealed a high roughness for the PEO coating. The chemical composition of coatings was determined using X-ray energy distribution spectroscopy (EDS), and the corrosion behavior of the AZ91 substrates with/without coating was studied by the potentiodynamic polarization test in the Ringer solution. The results showed that the corrosion (E_{corr}) potential of the AZ91 substrate increased compared to a single-layer PDMS coating from -1.48 to -1.47 V, and their corrosion current density (i_{corr}) reduced from 4.3 to 0.486 $\mu A \cdot cm^{-2}$ in the order given. However, by applying PEO coating as a pre-treatment utilizing the PEO/PDMS composite coating, these values were obtained -0.75 V and 0.9 $nA \cdot cm^{-2}$, respectively. So, applying PEO/PDMS hybrid coating may effectively reduce the high corrosion rates of magnesium alloys as the main limitations in the physiological environment.

Keywords AZ91 magnesium alloy · PEO coating · Polydimethylsiloxane · Corrosion resistance

1 Introduction

In recent years, numerous researches have focused on developing biodegradable and low-density bioimplants regarding higher strength. One of the new materials that meet these requirements is magnesium and its alloys [1]. Young's modulus (41–45 GPa) and density (1.74–2 $g \cdot cm^{-3}$) are close to human bones features (3–20 GPa and 1.8–2.1 $g \cdot cm^{-3}$), so

as the implant material, it can reduce the impact of stress shielding. They are also lighter than other biomedical metals. Also, magnesium is found naturally in bone composition and is one of the metals needed for metabolism. Therefore, due to these beneficial aspects, magnesium alloys have become an attractive subject of research as implants [2–5]. Despite the tremendous benefits, magnesium alloys' main limitation as biomedical materials is their high corrosion rates, including the release of hydrogen and alkaline environments that is a concerning issue for biomedical applications [3–6]. Surface modification is a promising approach to improve the performance of magnesium biological materials for orthopedic uses. There are a variety of surface modification methods such as conversion coatings, plasma electrolytic oxidation, electro-deposition, electrophoretic deposition, sol–gel coatings, polymer coatings, chemical vapor deposition, physical vapor deposition, sputtering, and ion implantation [7–10].

✉ Ali Doostmohammadi
Doost@yorku.ca

1 Department of Engineering, Shahrekord University, Shahrekord, Iran

2 Yekta Mobaddel Pars Co., Science and Technology Campus, Yazd University, 89158-18411 Yazd, Iran

3 Department of Mechanical Engineering, York University, BRG 433B, 4700 Keele St, Toronto, ON M3J 1P3, Canada

One of the surface modification methods that is always considered as an applicable measure is applying polymer coatings. Polymeric coatings are attractive for bio-applications as they protect against corrosion and other applications such as drug delivery and the ability to factor with organic biomolecules. Organic/polymeric coatings have great potential to prevent magnesium alloys' corrosion because these coatings provide a barrier layer between a corrosive environment and metal surface [6, 7, 9–11]. In recent years, various polymeric coatings including poly-lactic acid (PLA) [12], poly(L-lactic acid) (PLLA) [6], poly lactide-*co*-glycolide (PLGA) [13, 14], and poly(ε-caprolactone) (PCL) [6, 15, 16] were applied on pure magnesium, and different magnesium alloys substrates. Reported results have showed corrosion resistance, adhesion, and cellular growth have been improved [13–17].

Another method for surface modification of magnesium is the plasma electrolytic oxidation (PEO) or micro-arc oxidation (MAO) process that produces stable, hard, and resistant to abrasion and corrosion of coating. For orthopedic implants, PEO porous coating due to the reduction of corrosion rate and the utilization as pre-treatment to perform organic-based coatings has been highly regarded [8, 17]. The inappropriate bonding of the polymeric coating with the substrate has led to applying a PEO coating that provides appropriate bonding sites by using porosities for better adherence of polymeric coatings on the surface. An investigation reported that the MAO/CS composite coating has more corrosion resistance than single-layer MAO or chitosan coatings performed on Mg–Zn–Ca alloy [18].

In general, the condition of coating/substrate interfaces is a valid parameter in the degradation of coatings so that the metallurgical and chemical bonds at the interface can affect corrosion resistance. It has been reported that the metallurgical and chemical bonds in the coating/substrate interfaces for MAO/Mg and MAO/Chitosan have shown a significant impact on the improvement of the corrosion behavior of the alloy [19]. Also, an investigation showed improving the corrosion resistance of the AZ31 substrate with a double-layer coating of MAO/PLA in comparison with the substrate with a single-layer PLA coating can be only the result of two reasons; on the one hand, the porous MAO coating formed on the substrate may improve the thickness of the PLA layer resulting from the immersion coating process, and on the other hand, the MAO layer has improved adhesion between the PLA layer and magnesium substrate [20].

In many other studies, biodegradable polymers such as PLA, PLLA, CS, and other polymeric coatings were applied on different magnesium alloy substrates coated by PEO, and resistance to corrosion and biocompatibility of magnesium substrates were improved [18, 20–23]. Results revealed that the PMTMS polymer had been applied on an AZ31 surface, which had been modified by MAO coating showed better

corrosion resistance compared to MAO/PLA coating, due to greater sustainability and a physical barrier performance against a corrosive environment attack [24].

In this regard, poly(dimethylsiloxane), which is known as a type of organic/inorganic hybrid polymers because of low surface energy and good hydrophobicity, excellent corrosion resistance, biocompatibility, good thermal and oxide stability, and excellent chemical resistance, can be used for various applications, including protective coatings in biomedical applications [25–29]. Applying a single-layer polymer coating on metal surfaces has some challenges, and it does not provide relevant results. Hence, in the present study, we used the PEO process as surface modification and an interlayer coating to improve applying PDMS polymer coating on the Mg substrate.

2 Experimental procedures

2.1 Sample preparation

AZ91 alloy sheets with $20 \times 20 \times 3$ mm dimensions and chemical composition (wt%) of Al < 8.9, Zn < 0.62, Mn < 0.25, Si < 0.024, Sn < 0.013, Zr < 0.008, Fe < 0.005, Cu < 0.001, and balance Mg were used as substrate. The samples were ground by 600–3000 grits SiC abrasive papers to remove the surface pollution and achieve the uniform surface roughness. In this case, the surface roughness of 0.12 µm was formed on their surfaces. The samples were rinsed and washed in an ultrasonic bath with ethanol and distilled water for 10 min and eventually dried by a warm stream.

2.2 PEO treatment

PEO coating was performed in an alkaline aqueous electrolyte containing 6 g L^{-1} sodium silicate (($Na_2O)_x \cdot SiO_2$, 37 wt%), 2 g L^{-1} potassium fluoride (KF) and 8 g L^{-1} potassium hydroxide (KOH) and retention of pH above 12. Potassium hydroxide is a major component for pH control. It is also used to improve electrolyte conductivity, so potassium fluoride has been added to verify the electrical conductivity of the electrolyte and sodium silicate used to stabilize the arc during the PEO process [30, 31].

A digital pH Meter AZ instrument (8651 PH & ORP Meter) was used to measure the pH of the electrolyte. The electrical conductivity of the electrolyte was estimated at 13.6 mS cm^{-1} using the digital conductivity meter (JEN-WAY 4520). Figure 1 shows the used instruments for PEO coating. The cathode was a 316L stainless steel cylindrical container with a volume of 7 L, which is connected to the negative pole of the set-up. The samples were attached to the positive pole (anode) as a working electrode using a

Fig. 1 Schematic of applied plasma electrolytic oxidation (PEO) system for coating [32]
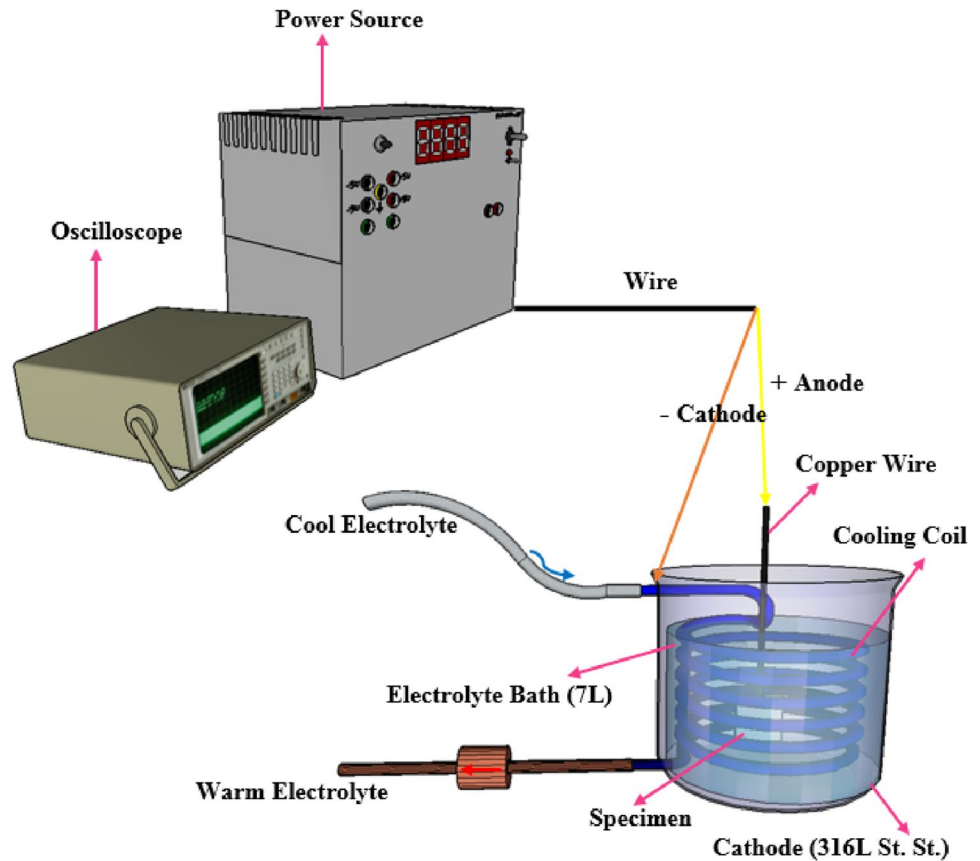
polymer-covered copper wire, and the samples were placed in the middle of the cathode container. The electrochemical cell was equipped with a submersible centrifugal electrical pump for electrolyte stirring. The cell was placed in a water-filled bath in which a chiller controlled its temperature. The external cell walls were adopted as the heat exchanger for cooling the electrolyte to keep the temperature at the range of 15 ± 1 °C. A digital thermometer Peak meter model TP500 manufacturing company HITSAN was utilized to measure the temperature of the electrolyte bath. A 700 V/30 A power source equipped with an IGBT-based pulser was employed for applying the pulsed current waveform. During the PEO process, the cell current–time responses were recorded by the power source, and a GPS 2024 digital oscilloscope was used to monitor the waveforms. The coating was performed under the unipolar waveform with a constant voltage of 440 V for 10 min with a duty cycle of 10% at the frequency of 1000 Hz. After the coating process with the PEO method, samples were washed with distilled water and dried by warm air blowing.

2.3 Polydimethylsiloxane coating process

3 g polydimethylsiloxane was added to 5 ml of toluene; then, a magnetic stirrer with a speed of 500 rpm for 20 min at a temperature of 45 °C was used to make a coating solution. At the beginning of the process, 0.3 g of the curing agent of dimethylsiloxane (with the weight ratio of PDMS: the curing agent = 10:1) was added to the above homogeneous solution, and the final solution was stirred for 30 min and at a speed of 500 rpm by a magnetic stirrer at the temperature of 60 °C to obtain a viscous and gel-like solution. The immersion method was used for the coating process. The AZ91 magnesium alloy substrate and the pre-treated sample's surface by PEO process were entered into the coating solution under the speed of 10 cm·min^{-1}. It was kept in solution for 3 min and then at the same speed of has brought outside and was placed at ambient temperature. Finally, the coated samples were placed in the dryer for 4 h at a temperature of 60 °C to apply the curing of the PDMS on the substrate. Samples after all coating processes were named AZ91, PDMS (bare magnesium alloy with a single-layer PDMS polymer coating), and PEO/PDMS sample (applying PDMS polymer coating on the surface after the PEO process).

2.4 Characterization

In order to study the phase composition of the coated and non-coated substrate, an X-ray diffraction test (XRD) was performed using an X-ray diffractometer (G.N.R X-Ray

Diffraction EXPLORER) (Cu Kα, $\lambda = 0.154186$ nm). X-ray diffraction patterns achieved in the voltage of 40 kV and the current of 30 mA in a range 2θ between 20° and 80° with the step size and a scan rate of 0.01° and 0.5 s, respectively. Results were analyzed by X'Pert HighScore Plus software. The surface and cross section morphology of coatings were investigated by field emission scanning electron microscopy (FESEM, TESCAN, MIRA3). To evaluate the coatings, first, the single-layer PEO coating and PEO/PDMS double-layer were sealed by epoxy resin. Then, the cross section surfaces were prepared by SiC sandpaper to the 3000 grit and polished. Also, the chemical composition of the coatings was examined by field emission scanning electron microscopy equipped with energy-dispersive X-ray spectroscopy (EDS). Topography and surface roughness of PEO coating were investigated by atomic force microscope (AFM). Also, for the characterization of the surface roughness, a roughness meter (Mitutoyo SJ.210) was used according to the ISO 1997. To evaluate and compare the corrosion behavior of the samples, the potentiodynamic polarization tests were applied in Ringer solution (with a combination of 0.86 g NaCl, 0.030 mg KCl, and 0.033 g CaCl$_2$, per 100 ml) and pH value of 7.4 at 37 °C using an AMETEK potentiostat/galvanostat (PGSTAT) (PARSTAT 2273). Electrochemical impedance spectroscopy (EIS) measurements were utilized to give a better explanation of coatings' performances in a corrosive environment. Tests were carried out at the frequency range of 100 mHz to 100 kHz, with a peak-to-peak amplitude of ± 10 mV versus OCP. Obtained EIS data were analyzed using ZView software to offer the best fit data and equivalent circuits. Also, polarization tests were performed with a 1 mV s^{-1} scanning rate. First, the samples were immersed for 2 h in the solution before the test achieved a stable mode. Then, the polarization curves (E-Log i) were obtained in the potential range of 300 mV versus the open

circuit potential (OCP). The polarization data were investigated by PowerSuite software. For all corrosion evaluation tests, a three electrodes cell, including a saturated calomel electrode (SCE) as a reference electrode, a graphite electrode as a counter electrode, and samples as a working electrode, was used. For each sample, the electrochemical tests were carried out in triplicate.

3 Results and discussion

3.1 Current density–time responses during the PEO process

Figure 2 shows the changes of current density versus time under constant voltage of 440 V for the substrate of AZ91 magnesium alloys in the electrolyte. In Fig. 2, four different stages with a variety of curve slope can be seen. The current density increases linearly with a very steep slope in stage I. This stage is related to the beginning of sparking and anodization process, in which a passive thin oxide film is formed on the metal surface [30–32]. In stage II, after reaching the constant voltage of 440 V and with the development of more plasma micro-arcs, a thicker PEO coating is formed, and the electrical resistance of the substrate increases. Therefore, according to Ohm's law, the current density decreases linearly with a very sharp slope [32]. In the third stage, a non-uniform and porous oxide layer develops. At this stage, continuous growth and breakdown of the oxide layer occur, so the growth of the oxide layer becomes slower and the current density decreases with a lower slope [32, 33]. In the last stage, by the formation of a compact PEO coating with a uniform structure, the breakdown voltage increases severely, and the dissolution of the coating occurs only in

Fig. 2 Current density–time responses during plasma electrolytic oxidation (PEO)
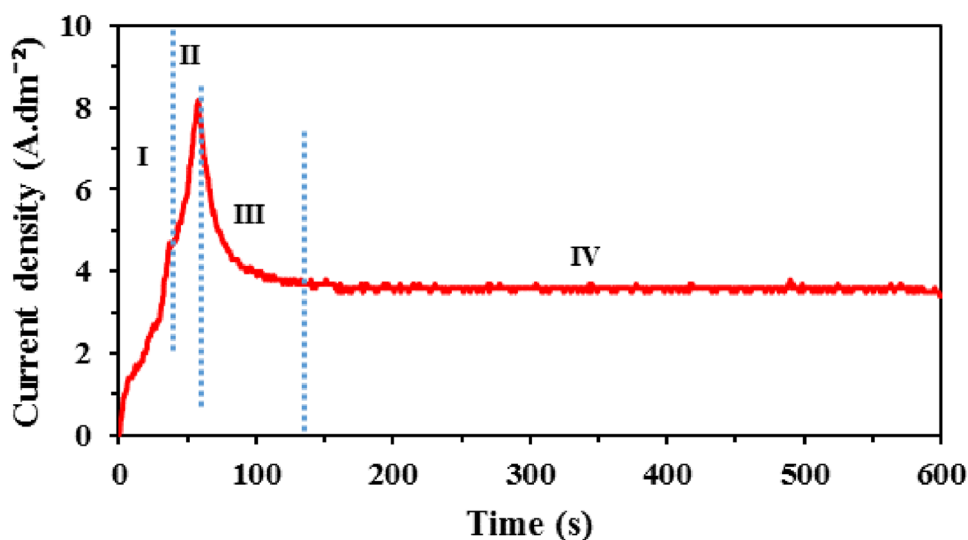
weaker areas. Therefore, the current density rate is almost constant [34].

3.2 Composition of the PEO coating

The X-ray diffraction patterns of AZ91 of magnesium alloy and PEO coating are shown in Fig. 3. As it is determined, the uncoated substrate is combined with Mg (JCPDS Card #00-004-0770) and $Mg_{17}Al_{12}$ (JCPDS Card #01-073-1148) phases. The X-ray pattern of coated sample on the AZ91 magnesium alloy substrate by PEO process demonstrates that the main phases include Mg_2SiO_4 (Forsterite, JCPDS Card #01-074-1678), $MgSiO_3$ (Clinoenstatite, JCPDS Card #01-077-2087), and MgO (Periclase, JCPDS Card #01-075-1525), as well as Mg peaks, which are also observed.

Such phases are in accordance with the research on the application of PEO coating on magnesium substrate in silicate electrolyte [35, 36]. Due to the porous nature of PEO coatings and X-ray penetration in the substrate, the magnesium of the substrate is observed in the pattern. The presence of magnesium peaks in the X-ray diffraction pattern of PEO coatings has been reported in other studies [37, 38]. Because of the rapid solidification of the molten oxide through sparking during the PEO process near the surface in contact with the aqueous electrolyte, the outer layer of the coating is formed from the amorphous phases due to having more faster solidification than the inner layer. The formation of amorph phases is also visible in the diffraction pattern of PEO oxide coating. Phase forming mechanism is as follows:

Initially, magnesium from the substrate and oxygen contained within the electrolyte are ionized at high voltages and converted to Mg^{2+} and O^{2-}, respectively. Hence, the MgO phase is produced by external migration of Mg^{2+} ions from the substrate to the oxide coating/electrolyte interface and internal movement of Mg^{2+} ions from the electrolyte toward the coating/substrate interface simultaneously, under the high localized temperature in the discharge channels due to applied electric field (at high voltage). The presence of Mg_2SiO_4 and $MgSiO_3$ shows the anions inside the electrolyte are widely involved in the coating's formation reactions.

Sodium silicate can be easily hydrolyzed and then form $Si(OH)_4$ in an aqueous electrolyte. Because of the high temperature of the plasma micro-discharges, $Si(OH)_4$ is dehydrated and converted to SiO_2 and then reacts with the molten MgO and because of contact with the electrolyte and produces a combination of MgO and Mg_2SiO_4 phases. On the other hand, Mg^{2+} and ions react with each other during the PEO process and produce $MgSiO_3$ and Mg_2SiO_4 according to Eqs. (1) and (2).

$$Mg^{2+} + SiO_3^{2-} \rightarrow MgSiO_3 \tag{1}$$

$$2Mg^{2+} + SiO_3^{2-} + 2OH^- \rightarrow Mg_2SiO_4 + H_2O \tag{2}$$

Fig. 3 XRD patterns of AZ91 of magnesium alloy and PEO coating
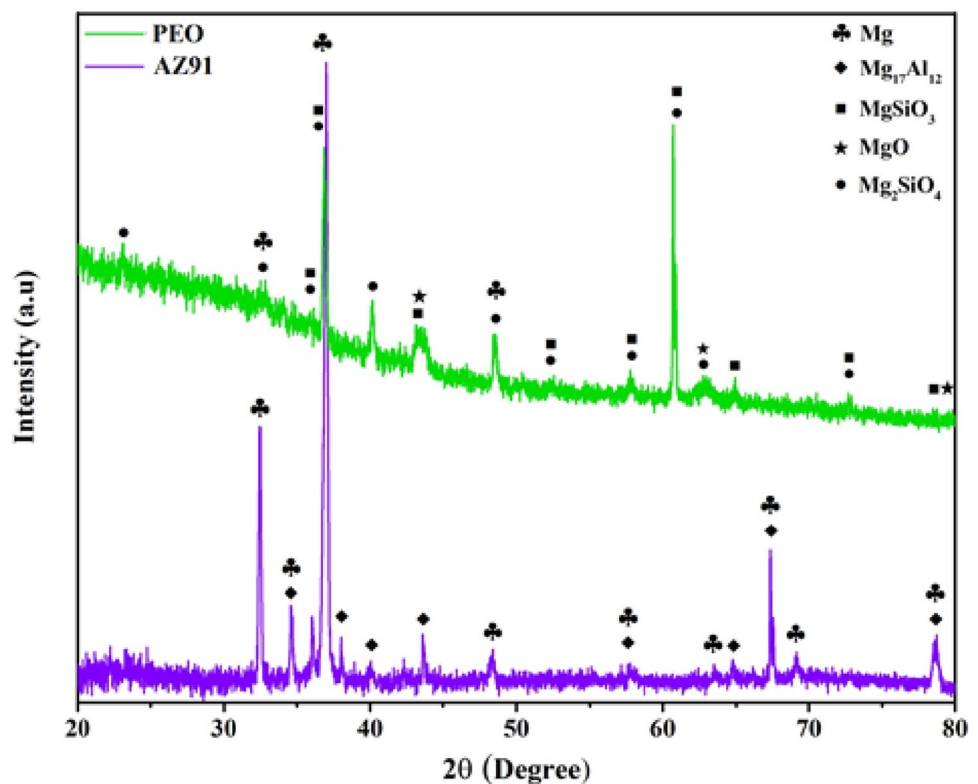
The lower amount of $MgSiO_3$ than Mg_2SiO_4 demonstrates that mainly the formation of the $MgSiO_3$ phase in the early stages of the PEO process has been taken. Subsequently, in the next step of the PEO process, $MgSiO_3$ has a react with MgO under high-temperature conditions and forms Mg_2SiO_4 [35, 39].

As explained before, ions enter to discharges channels and participate in the reactions; thereby, the oxides containing the elements of the substrate and electrolyte are formed, and the coating is produced. In the X-ray diffraction pattern of the PEO coating, the MgF_2 phase could not be observed that can be attributed to two reasons: (a) The amount of MgF_2 has been less than XRD detection, and (b) the location of the fluorine element accumulation is in the substrate/coating interface, and this phase could not be detected, so it is probably possible to prove the presence of MgF_2 phase by increasing the time of each step size in XRD test.

3.3 Surface and cross section morphology of coatings

Figure 4 shows the net-like (scaffold) surface morphology of the PEO coating formed on the substrate of AZ91 magnesium alloy. The PEO coating surface contains a network of micropores, micro-cracks, and oxide granules. This morphology is commonly observed for PEO coatings deposited on magnesium alloys in a silicate electrolyte [32, 38]. Due to the continuous discharges and breakdown of the coating layers during the oxidation process, and the egress of trapped gases from the discharge channels, micropores are formed, and the diameter of these micropores is estimated in the range of 0.5–5 µm [34, 40]. Also, because of the rapid solidification of molten oxide and thermal stresses as a result of different thermal coefficients of the oxide coating and substrate, micro-cracks are created [21, 34, 35]. Also, due to high temperature and local pressure in the PEO process, molten metal and ions of electrolyte react in the discharge channels, and then, produced molten products are removed from the discharge channels. After relatively fast cooling, these products accumulate around the discharge channels

Fig. 4 **a**, **b** FESEM observation of PEO coating's surface morphology on AZ91 magnesium alloy, and **c** three-dimensional surface plots by AFM
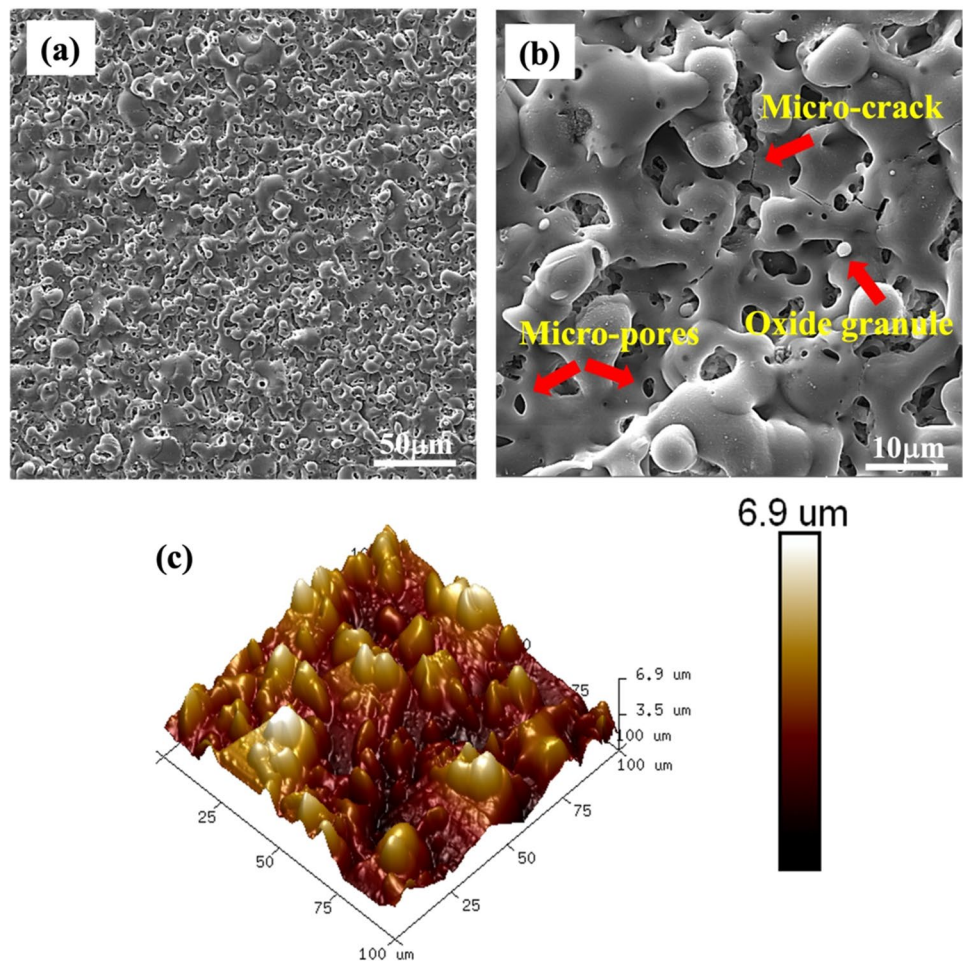
and lead to the production of the pancake morphology [23, 41–43].

Figure 4c illustrates the AFM three-dimensional surface morphology of PEO coating. Ununiform morphology shows the porous structure of the PEO coating for electrical discharge carrying out during the PEO process. The mean surface roughness (Rq) of PEO coating obtained by the atomic force microscope was measured by about 1 micron (993 nm). Also, the roughness value derived from the surface of the coating was about 1.2 μm (1.29 ± 0.08).

Figure 5 shows X-ray energy distribution spectroscopy (EDS) results of the PEO coating's surface. The results indicate that this coating is mainly of oxygen (48.72 wt%), magnesium (31.6 wt%), and silicon (13.96 wt%) and approves the detection of MgO, $MgSiO_3$, and Mg_2SiO_4 compounds in the X-ray diffraction patterns. As mentioned, the magnesium element of substrate and the components of electrolyte such as silicon and oxygen play a essential role in the formation of oxide coating in the PEO process.

Figure 6 demonstrates the cross section FESEM observation of the PEO coating. As Fig. 6b, a thick ceramic coating (16.5 ± 2.7 μm) which is grown on magnesium alloy surface consists of two layers, a thin inner layer (barrier layer), which is adjacent to the substrate with the maximum thickness of 1–2 μm and provides excellent adhesion between the coating and substrate [21, 39, 41, 42, 44]. The second layer is the outer porous layer, which consists of a significant part of the PEO coating [31, 35, 43].

Production of the oxide layer created during the PEO process grows in both directions, inward to magnesium

alloy substrate and outward to the coating's surface, concurrently [21, 32, 41]. The formation of a wavy coating/substrate interface can result from the α-Mg dissolution during the PEO process and the introduction of β-$Mg_{17}Al_{12}$ as an intermetallic phase on the grain boundaries. Since no discontinuities are observed between the coating and substrate, the coating is well adhering to the substrate [21, 32, 41, 42]. Since micropores affect the corrosion behavior, only the outer layer consists of porosities, and there are no pores in the dense inner layer, so it is logical to conclude that the dense inner layer has excellent performance against corrosive environments [31, 32, 45].

Figure 7 represents the FESEM cross section of the PEO coating along with the map distribution elements. Magnesium is distributed from the substrate and silicon of the electrolyte, along with oxygen evenly throughout the coating, which confirms the simultaneous presence of the substrate and electrolyte elements in the formation of phases within the oxide layer of PEO coating. Also, as seen, the fluorine ions accumulate at the interface, which represents the migration of fluorine ions from the electrolyte toward the coating/substrate interface through intense sparks taken during the process of PEO.

The results reveal that this coating is mainly composed of oxygen, magnesium, and silicon, indicating the presence of compounds determined in the X-ray diffraction pattern of PEO coating, and approves the presence of MgO, $MgSiO_3$, and Mg_2SiO_4 phases. As mentioned before, plasma electrolyte oxidation is a process by which the substrate's elements and electrolyte bath play a significant role in creating oxide

Fig. 5 EDS analysis of the surface of PEO coating fabricated on AZ91 magnesium alloy in silicate electrolyte
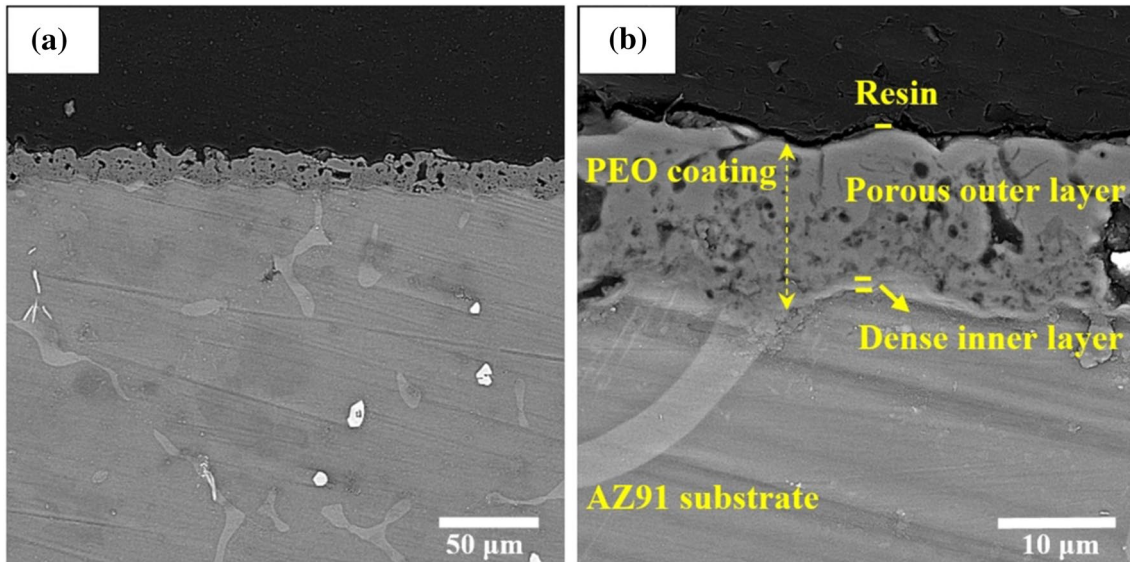

Element	(Wt.%)
O	48.72
Mg	31.60
Si	13.96
F	3.42
Al	1.53
K	0.41
Na	0.36
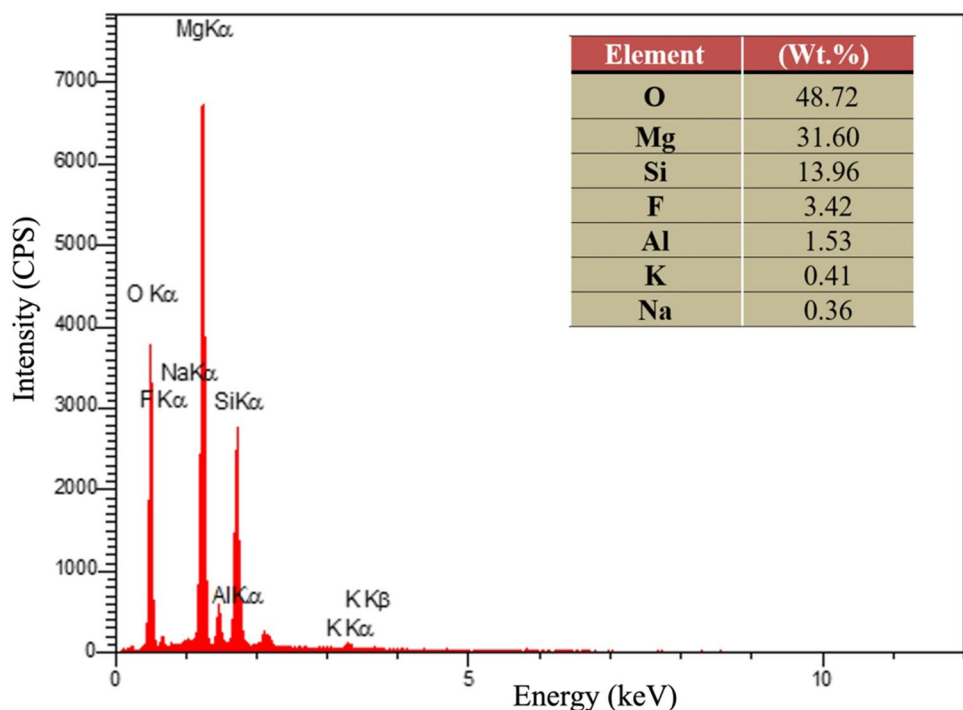
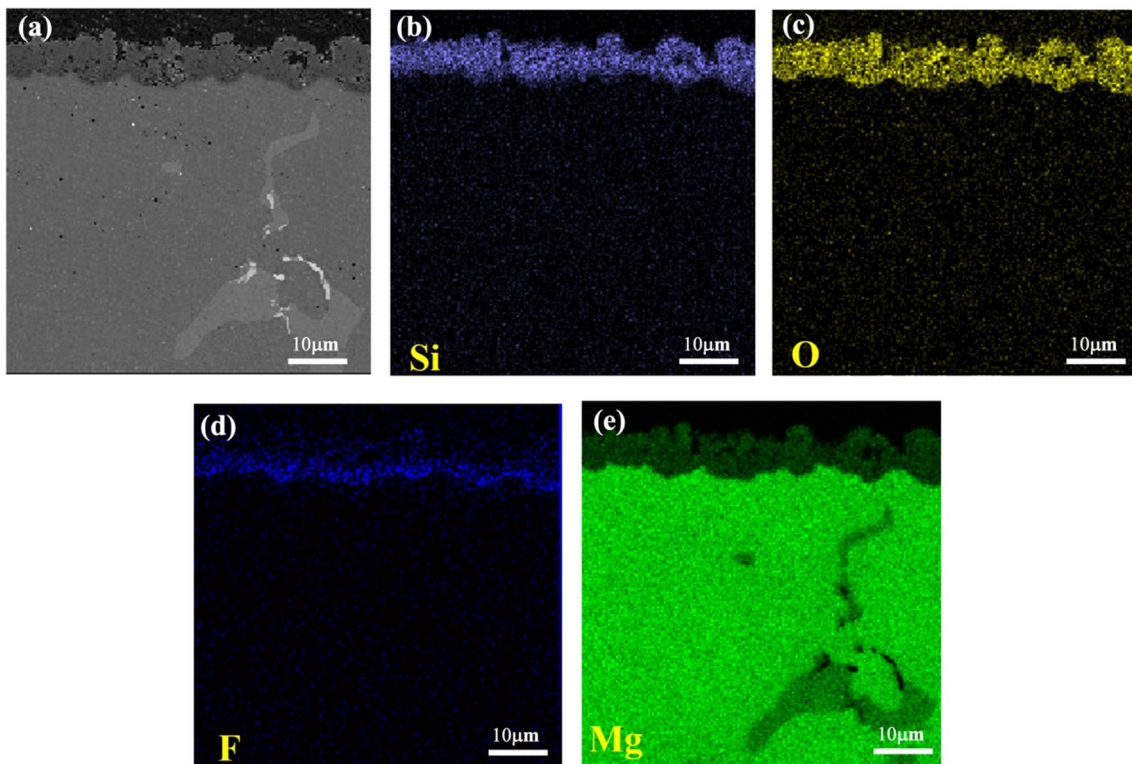**Fig. 6** FESEM cross section images of the PEO coating

**Fig. 7** Cross section and elemental distribution map of PEO coating

coating. So, it is clear that magnesium element from the substrate and silicon and oxygen elements from the electrolyte have been involved in forming this oxide layer.

Figure 8 illustrates the FESEM surface morphology and cross section of the polymeric coating of polydimethylsiloxane on the substrate of AZ91 magnesium alloy modified by the PEO process. A thick PDMS layer with a thickness of 12.5 ± 0.3 μm was produced on the PEO coating. The surface of the polymer coating is free of any cracks and pores and is completely smooth and uniform, and

Fig. 8 Surface and cross section FESEM observations of the PEO/PDMS coating
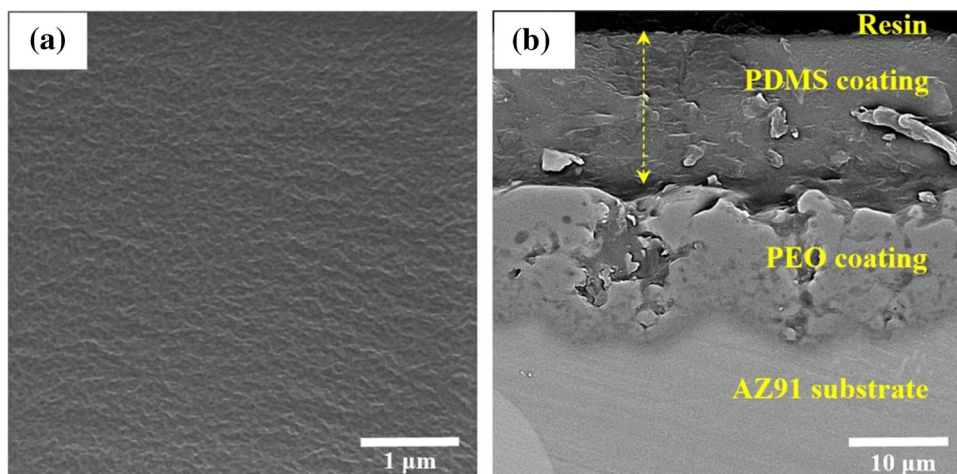
the micropores and micro-cracks belonging to the surface of the PEO coating are fully covered.

For better evaluation of elements distribution of the PEO/PDMS sample, the elemental map is shown in Fig. 9. Since the PDMS is a silicon polymer and its main chain is made from the repetition of silicon bonds to oxygen, and its side chain is also made from methyl groups (–CH₃) [26], so the presence of silicon, oxygen, and carbon elements is the characteristic of the existence of silicones in the coating. The result of the elemental distribution map for the carbon shows the presence of the carbon element in the PEO coating clearly, which reflects the penetration of the PDMS coating into the micro-pores and micro-cracks of the PEO coating that can result in a good physical binding and adhesion of this polymer coating to PEO coating [20, 21, 23, 24]. As seen, even the penetration of silicon element into the micropores of the PEO is visible.
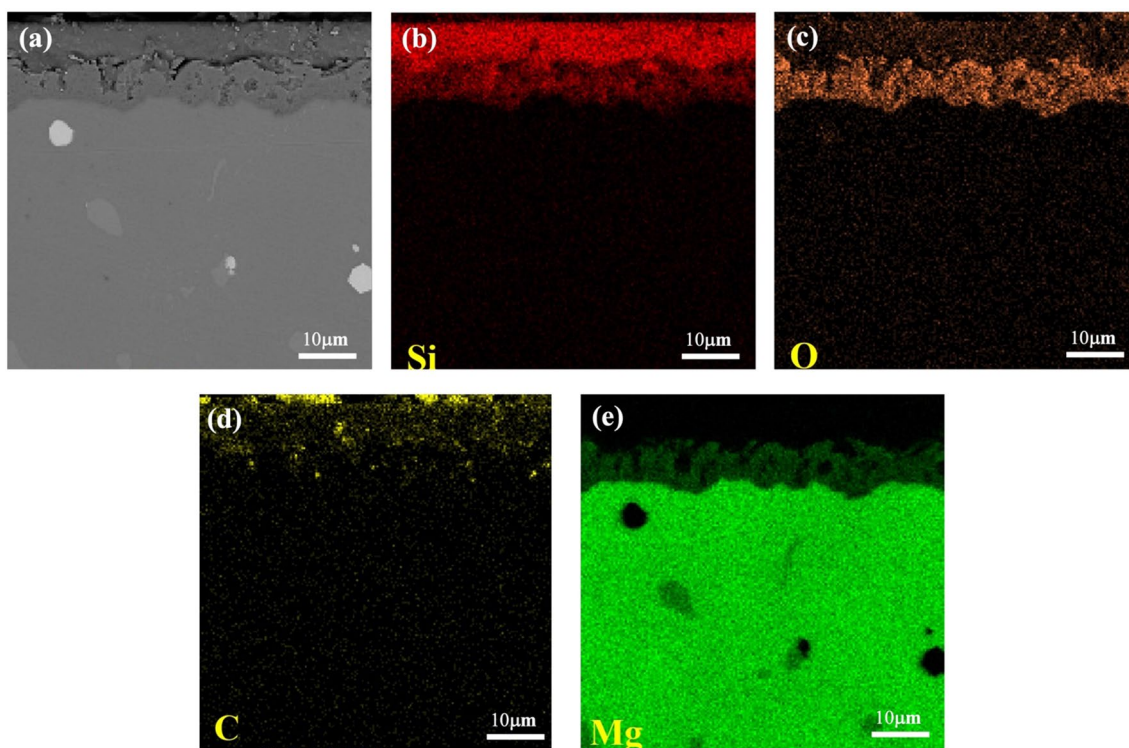
Fig. 9 Cross section and elemental maps of PEO/PDMS coating

3.4 Electrochemical measurements

3.4.1 Electrochemical impedance spectroscopy (EIS) evaluations

Due to the high corrosion rate of Mg, the use of Mg-based implants in biomedical is almost impossible [46]. Therefore, the surface of Mg was modified with coatings of PDMS and PEO/PDMS. So the corrosion behavior of the coatings was determined using EIS tests after 2 h immersion in the Ringer solution at pH 7.4 and 37 °C. Figure 10 illustrates Nyquist and Bode plots of uncoated and coated AZ91 Mg alloy samples. The Nyquist diagram shows a capacitive loop for the AZ91substrate which is related to the reaction between the electrolyte and the Mg substrate and the formation of a double-layer capacitor (Fig. 10a). For the PDMS coating, the Nyquist diagram shows two semicircles (Fig. 10a). Also, two time constants are seen clearly in the Bode-phase diagram for this coating (Fig. 10b). At low frequencies, CPE_{dl} and R_{ct} show the interfacial reaction between Mg substrate and PDMS coating, and R_{ct} indicates the diffusion of corrosive agents on the substrate surface [47]. According to the Nyquist diagram, the corrosion performance of PDMS coating has improved about 5 times compared to Mg substrate. To increase the corrosion resistance of the Mg substrate, the surface of the substrate was modified by the PEO process, and then, the PDMS coating was applied on the surface.

According to the Bode-phase diagram in Fig. 10c, PEO/PDMS coating displays three time constants. At high frequency, the first semicircle and time constants correspond to PDMS coating and the outer porous of the PEO coating [48]. The next time constant at medium frequencies is related to the inner dense layer of the PEO coating [48, 49]. The last time constant refers to the charge transfer resistance of the Mg substrate and the interfacial reaction between the Mg substrate and the PEO coating [48]. As can be seen in the Nyquist diagram, the corrosion resistance of PEO/PDMS coating has increased dramatically compared to the Mg substrate and PDMS coating. These results can be attributed to the filling of micropores and micro-cracks of PEO coating and the surface sealing by PDMS coating [20].

The equivalent circuits are used to fit the EIS data of the different samples (Fig. 11), and the fitting data are listed in Table 1.

Where R_s is the uncompensated resistance of the solution, and R_{ct} and CPE_{dl} are resistance and the capacity of double-layer charge transfer for AZ91 alloy, respectively. R_{out} and CPE_{out} are outer layer resistance and non-ideal capacitor or constant phase element, and R_{in} and CPE_{in} are inner layer resistance and constant phase element of the PEO coating. For PDMS and PEO/PDMS samples, R_{pc} and CPE_{pc} represent polymer coating resistance and constant phase element, respectively.
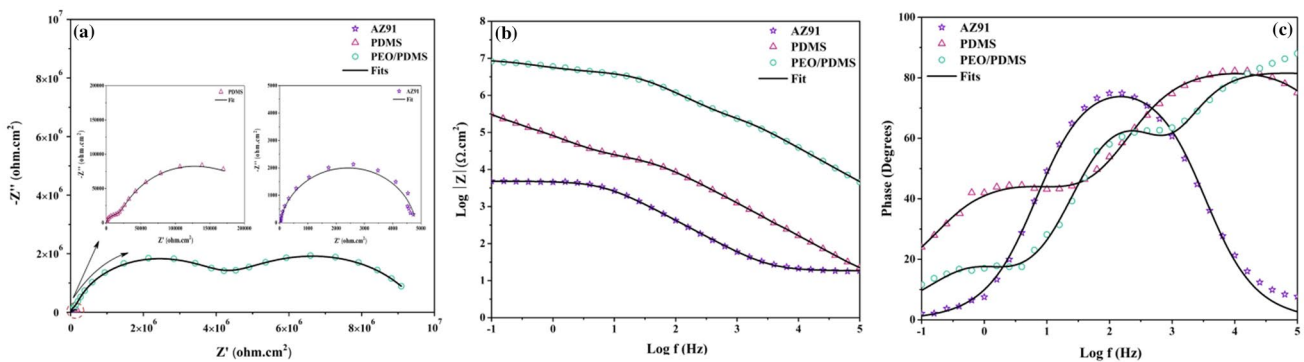

Fig. 10 **a** Nyquist, **b** Bode Z, and **c** Bode-phase plots obtained through EIS evaluation after 2 h of immersion in Ringer solution at pH 7.4 and 37 °C
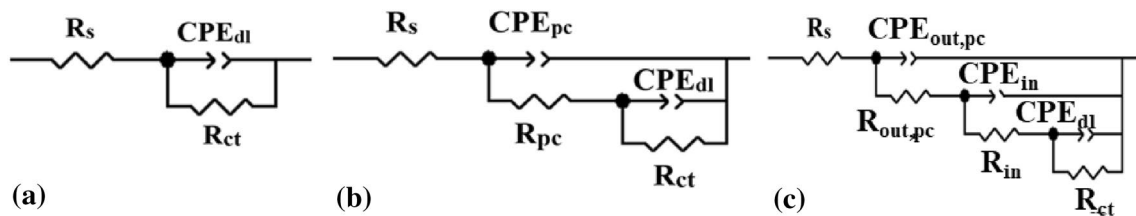

Fig. 11 Equivalent circuits applied to fit the impedance data of **a** AZ91, **b** PDMS [47], and **c** PEO/PDMS samples [48]

Table 1 Fitting results of the EIS data in Fig. 10 using equivalent circuits in Fig. 11

Sample	CPE$_{dl}$ (μF cm^{-2} s^{n-1})	R$_{ct}$ (kΩ·cm²)	CPE$_{out}$ (μF cm^{-2} s^{n-1})	CPE$_{in}$	CPE$_{pc}$	n$_{out}$	n$_{in}$	n$_{pc}$	R$_{out}$ (MΩ·cm²)	n$_{dl}$	R$_{in}$	R$_{pc}$
AZ91	7.14±0.05	4.80±0.15	–	–	–	–	–	–	–	0.9±0.02	–	–
PDMS	1.7±0.03	213.97±0.53	–	–	0.223±0.03	–	–	0.88±0.03	–	0.91±0.02	–	0.025±0.0002
PEO/PDMS	0.003±0.0001	3950±50	0.0001±0.00002	0.971±0.03	–	0.74±0.04	0.98±0.02	–	5.610±0.06	0.88±0.03	0.0186±0.0003	–

The results of Table 1 show an increase in corrosion resistance of PDMS and PEO/PDMS samples compared to the AZ91 substrate. The corrosion resistance of AZ91 substrate, PDMS and PEO/PDMS coating is 4.8 kΩ·cm² to about 0.239 MΩ·cm² and 9.56 MΩ·cm², respectively.

3.4.2 Polarization results

The potentiodynamic polarization test was carried out to investigate the corrosion behavior of different samples (AZ91 magnesium alloy substrate, PDMS coating sample, and PEO/PDMS hybrid coating) in Ringer solution at a temperature of 37 °C. Figure 12 represents the curves obtained from the polarization test.

The corrosion potential (E_{corr}) and corrosion current density (i_{corr}) extracted from the plots are reported in Table 2. Also, the polarization resistance (R_P) of samples were determined by the Stern–Geary equation (Eq. 3):

$$R_P = \frac{\beta_a \beta_c}{2.303 i_{corr}(\beta_a + \beta_c)} \tag{3}$$

where β_a and β_c are anodic and cathodic slopes of polarization curves and improved corrosion resistance can be estimated by increasing the potential of corrosion, while the current density is reduced. High corrosion potential and low corrosion current density of coatings indicate a low corrosion rate besides more uniform corrosion and high corrosion resistance function [20]. In general, the more positive potential of corrosion (E_{corr}), the more corrosion resistance of coatings. Typically, the current density of corrosion (i_{corr}) is used to evaluate the kinetics of corrosion reactions, and the less current density of corrosion, the fewer corrosion rates, as well [20, 23].

As the results of Table 2, it is clear that all coatings have increased the corrosion resistance of the substrate. The corrosion potential of the sample has a single layer of PDMS compared to the bare AZ91 substrate has increased about 10 mV. Also, the current density of corrosion for AZ91 and PDMS samples has fallen from 4.3 to 0.486 μA·cm^{-2}, respectively. For the PEO/PDMS sample, a notable reduction of i_{corr} (0.9 nA·cm^{-2}) and a significant increase in E_{corr} (− 0.75 V) have been observed. A noticeable decrease of the i_{corr} for the sample of hybrid PEO/PDMS coating in comparison with the substrate without coating and the surface with a single-layer PDMS coating can be related for two reasons; (1) the porous PEO layer has improved the physical and mechanical bonding between the PDMS coating and magnesium substrate, which results in accordance with former investigations [20]; and (2) the PDMS polymer coating fills the porous structure of the PEO coating and prevents the penetration of the Ringer solution toward the substrate, which has been reported in previous studies [20–24].

Fig. 12 Polarization curves of the AZ91 substrate and coated samples after 2 h of immersion in Ringer solution at pH 4 and 37 °C
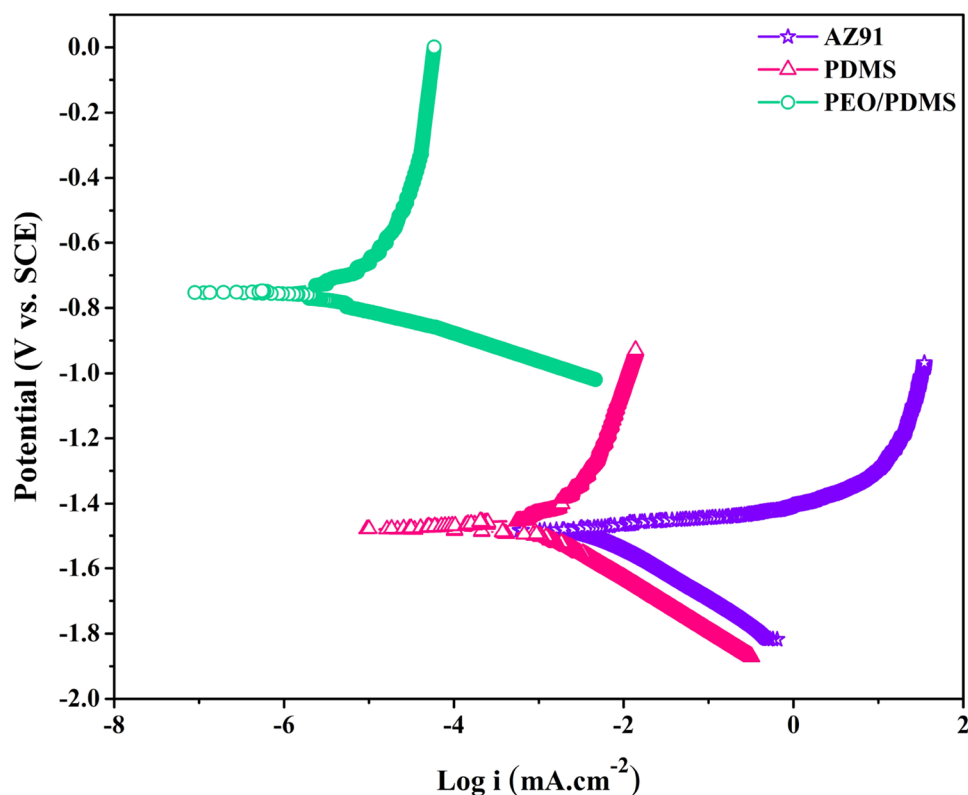
Table 2 Electrochemical data extracted from the potentiodynamic polarization curves in Fig. 12

Sample	E_{corr} (mV vs. SCE)	i_{corr} (nA·cm^{-2})	β_a (mV dec^{-1})	β_c	R_P (MΩ cm^2)
AZ91	− 1482 ± 14.7	4344 ± 235.4	27.3 ± 2.2	152 ± 16.3	0.0023 ± 0.0002
PDMS	− 1468.3 ± 18.4	486 ± 81.8	104.2 ± 5.3	70 ± 21.9	0.0374 ± 0.008
PEO/PDMS	− 751.3 ± 8.7	0.931 ± 0.21	63 ± 12.4	48 ± 5.7	13.143 ± 2.008

The cathodic polarization curves indicate hydrogen release in the cathode, while the anodic polarization curves represent the dissolution of magnesium into the solution [20]. As shown, it is clear that the hybrid PEO/PDMS coating has a passivation area rather than two other samples that can be attributed to the presence of a dense, uniform, and non-porous polymer coating on the surface. Such behavior indicates the fact that the surface of the substrate has become utterly passive because of the presence of this protective layer (polymer coating) on the substrate. Another factor important in the potentiodynamic polarization test is the polarization resistance (R_p), which directly relates to corrosion resistance. Calculated values for the polarization resistance reveal that coated samples' polarization resistance is higher than the bare substrate. The corrosion resistance of the PEO/PDMS sample has increased dramatically to about 13.143 MΩ·cm^2 that is a significant amount for a coated magnesium substrate.

The corrosion potential of the AZ91 magnesium alloy substrate has increased from − 1.48 to − 0.75 V by applying a PEO/PDMS hybrid coating. In contrast, the current density of the corrosion (i_{corr}) for PEO/PDMS has decreased approximately 4778 times. Therefore, it can be expected that the PEO/PDMS hybrid coating may reduce the main limitations of magnesium alloys considerably, i.e., their high corrosion rate in physiological environments such as body fluids.

4 Conclusion

PEO/PDMS hybrid coating was fabricated on AZ91 magnesium alloy using plasma electrolytic oxidation coupled with the PDMS polymer layer. A ceramic oxide layer of MgO was produced on AZ91 alloy with a thickness of about 16.5 ± 2.7 μm through the PEO process, and the PDMS coating as a sealing layer in the thickness of about 12.5 ± 0.3 μm

was performed using the immersion method. The results of the elemental distribution map for samples indicate the penetration of the PDMS into the defects of the PEO coating (micropores and micro-cracks) that can lead to an excellent physical binding and adhesion between the PDMS layer and PEO coating. The PDMS coating produced a significant enhancement in the corrosion behavior of AZ91 alloy with PEO coating in Ringer. The data obtained from polarization tests indicate the i_{corr} of the PEO/PDMS sample is about 540 and 4778 times lower than PDMS and AZ91 samples, respectively. The impendence resistance of hybrid coating of PEO/PDMS is approximately 40 and 1991 times higher than PDMS coating and bare AZ91 alloy. Therefore, composite coatings with high corrosion resistance in the corrosive solution can be considered as a surface modification method to reduce the magnesium alloy's degradation rate in body fluids.

References

1. R. Radha, D. Sreekanth, J. Magnes. Alloys **5**, 286 (2017)
2. S. Heise, T. Wirth, M. Höhlinger, Y.T. Hernández, J.A.R. Ortiz, V. Wagener et al., Surf. Coat. Technol. **344**, 553 (2018)
3. X. Liu, Q. Yang, Z. Li, W. Yuan, Y. Zheng, Z. Cui et al., Appl. Surf. Sci. **434**, 1101 (2018)
4. G. Song, Corros. Sci. **49**, 1696 (2007)
5. Y. Yang, C. Michalczyk, F. Singer, S. Virtanen, A.R. Boccaccini, Appl. Surf. Sci. **355**, 832 (2015)
6. L. Xu, A. Yamamoto, Colloids Surf., B. **93**, 67 (2012)
7. H. Hornberger, S. Virtanen, A. Boccaccini, Acta Biomater. **8**, 2442 (2012)
8. T.S. Narayanan, I.S. Park, M.H. Lee, Prog. Mater. Sci. **60**, 1 (2014)
9. G.E.J. Poinern, S. Brundavanam, D. Fawcett, Am. J. Biomed. Eng. **2**, 218 (2012)
10. G. Wu, J.M. Ibrahim, P.K. Chu, Surf. Coat. Technol. **233**, 2 (2013)
11. Y. Zheng, X. Gu, F. Witte, Mater. Sci. Eng. R Rep. **77**, 1 (2014)
12. A. Alabbasi, S. Liyanaarachchi, M.B. Kannan, Thin Solid Films **520**, 6841 (2012)
13. J. Li, P. Cao, X. Zhang, S. Zhang, Y. He, J. Mater. Sci. **45**, 6038 (2010)
14. N.J. Ostrowski, B. Lee, A. Roy, M. Ramanathan, P.N. Kumta, J. Mater. Sci.: Mater. Med. **24**, 85 (2013)
15. J. Degner, F. Singer, L. Cordero, A.R. Boccaccini, S. Virtanen, Appl. Surf. Sci. **282**, 264 (2013)
16. H.M. Wong, K.W. Yeung, K.O. Lam, V. Tam, P.K. Chu, K.D. Luk et al., Biomaterials **31**, 2084 (2010)
17. G.B. Darband, M. Aliofkhazraei, P. Hamghalam, N. Valizade, J. Magnes. Alloys **5**, 74 (2017)
18. C. Yu, L.-Y. Cui, Y.-F. Zhou, Z.-Z. Han, X.-B. Chen, R.-C. Zeng et al., Surf. Coat. Technol. **344**, 1 (2018)
19. K. Bai, Y. Zhang, Z. Fu, C. Zhang, X. Cui, E. Meng et al., Mater. Lett. **73**, 59 (2012)
20. P. Shi, B. Niu, E. Shanshan, Y. Chen, Q. Li, Surf. Coat. Technol. **262**, 26 (2015)
21. H. Bakhsheshi-Rad, E. Hamzah, R. Ebrahimi-Kahrizsangi, M. Daroonparvar, M. Medraj, Vacuum **125**, 185 (2016)
22. P. Lu, L. Cao, Y. Liu, X. Xu, X. Wu, J. Biomed. Mater. Res. Part B Appl. Biomater. **96**, 101 (2011)
23. X. Xu, P. Lu, M. Guo, M. Fang, Appl. Surf. Sci. **256**, 2367 (2010)
24. L.-Y. Cui, S.-D. Gao, P.-P. Li, R.-C. Zeng, F. Zhang, S.-Q. Li et al., Corros. Sci. **118**, 84 (2017)
25. A. Blau, A. Murr, S. Wolff, E. Sernagor, G. Iurilli et al., Biomaterials **32**, 1778 (2011)
26. U. Eduok, O. Faye, J. Szpunar, Prog. Org. Coat. **111**, 124 (2017)
27. A. Francis, R. Detsch, A. Boccaccini, Ceram. Int. **42**, 15442 (2016)
28. S.H. Kim, J.-H. Moon, J.H. Kim, S.M. Jeong, S.-H. Lee, Biomed. Eng. Lett. **1**, 199 (2011)
29. J. Li, X. Liu, J.M. Crook, G.G. Wallace, Colloids Surf., B. **159**, 386 (2017)
30. A. Ghanbari, A.B. Khiabani, A. Zamanian, B. Yarmand, M. Mozafari, Mater. Today: Proc. **5**, 15677 (2018)
31. D.Y. Hwang, Y.M. Kim, D.-Y. Park, B. Yoo, D.H. Shin, Electrochim. Acta. **54**, 5479 (2009)
32. M. Rahmati, K. Raeissi, M.R. Toroghinejad, A. Hakimizad, M. Santamaria, Coatings **9**, 688 (2019)
33. M. Kaseem, H.-C. Choe, J. Alloys Compd. **819**, 153038 (2020)
34. A. Toulabifard, M. Rahmati, K. Raeissi, A. Hakimizad, M. Santamaria, Coatings **10**, 937 (2020)
35. S.L. Aktuğ, S. Durdu, I. Kutbay, M. Usta, Ceram. Int. **42**, 1246 (2016)
36. A. Seyfoori, S. Mirdamadi, A. Khavandi, Z.S. Raufi, Appl. Surf. Sci. **261**, 92 (2012)
37. H. Chen, G. Lv, G. Zhang, H. Pang, X. Wang, H. Lee et al., Surf. Coat. Technol. **205**, S32 (2010)
38. Z. Li, Y. Yuan, X. Jing, J. Alloys Compd. **541**, 380 (2012)
39. D. Chen, R. Wang, Z. Huang, Y. Wu, Y. Zhang, G. Wu et al., Appl. Surf. Sci. **434**, 326 (2018)
40. A. Heydarian, M. Atapour, A. Hakimizad, K. Raeissi, Surf. Coat. Technol. **383**, 125235 (2020)
41. R. Hussein, X. Nie, D. Northwood, Electrochim. Acta. **112**, 111 (2013)
42. R. Hussein, D. Northwood, X. Nie, J. Alloys Compd. **541**, 41 (2012)
43. C. Liu, J. Liang, J. Zhou, Q. Li, Z. Peng, L. Wang, Surf. Coat. Technol. **304**, 179 (2016)
44. R.-C. Zeng, W.-C. Qi, Y.-W. Song, Q.-K. He, H.-Z. Cui, E.-H. Han, Front. Mater. Sci. **8**, 343 (2014)
45. S. Durdu, A. Aytac, M. Usta, J. Alloys Compd. **509**, 8601 (2011)
46. F. Peng, D. Wang, D. Zhang, B. Yan, H. Cao, Y. Qiao et al., ACS Biomater. Sci. Eng. **4**, 4112 (2018)
47. Y. Shen, K. Li, H. Chen, Z. Wu, Z. Wang, Chem. Eng. J. **413**, 127455 (2021)
48. M. Toorani, M. Aliofkhazraei, M. Mahdavian, R. Naderi, Corros. Sci. **169**, 108608 (2020)
49. R. Aliramezani, K. Raeissi, M. Santamaria, A. Hakimizad, Surf. Coat. Technol. **329**, 250 (2017)